Journal of The Electrochemical Society, **149** (7) B321-B327 (2002)
0013-4651/2002/149(7)/B321/7/$7.00 © The Electrochemical Society, Inc.

Formation and Microstructures of Anodic Alumina Films from Aluminum Sputtered on Glass Substrate

S. Z. Chu,[z] K. Wada, S. Inoue, and S. Todoroki

National Institute for Materials Science, Advanced Materials Laboratory, Tsukuba, Ibaraki 305-0044, Japan

A transparent porous alumina nanostructure was formed on a glass covered tin-doped indium oxide (ITO) substrate by anodization of a highly pure sputtered aluminum layer. Details of the fabrication and microstructures of porous anodic alumina films are described and a possible mechanism of anodization is outlined. The variation of anodic current density reflects three processes, *i.e.*, (*i*) anodization of the sputtered aluminum layer, (*ii*) transition of electrolysis from aluminum to the underlying ITO film, and (*iii*) electrochemical reactions on the ITO film beneath the anodic alumina film. As all the aluminum is completely anodized, the resultant oxide films on the ITO/glass substrate possess a parallel porous structure (ϕ80-100 nm, cell size in ~350 nm) with a thin arched barrier layer (~80 nm) and exhibit a high transmittance in the ultraviolet-visible light range (75-100% transmittance 300-900 nm).
 [DOI: 10.1149/1.1480017]

Manuscript submitted August 13, 2001; revised manuscript received January 31, 2002. Available electronically May 9, 2002.

Porous anodic alumina, which consists of fine, uniform pores of nanometer dimension, has recently attracted increasing interest as a key material for the fabrication of various nanostructures.[1-5] The key feature of porous anodic alumina films is the uniform pore sizes, high pore density, and high aspect ratio which are difficult to obtain by conventional lithographic techniques. The formation process, microstructures, and properties of porous anodic alumina from thermomechanically prepared aluminum have been studied for many years and have been well documented in many books[6-7] and papers.[8-14] Porous anodic alumina is usually formed through anodizing bulk aluminum plates or foils at constant voltage or current density in various acidic electrolytes such as sulfuric, oxalic, phosphoric, chromic, citric acid, etc.[8-12] The dimensions of pores and unit cell of anodic oxide films are controlled readily by appropriate choice of anodizing solutions, voltage or current density, temperature,[8-12] or a pre-indentation process,[13] etc. For some special purposes, porous anodic alumina films are separated from the aluminum substrate[14] and used as templates to synthesize various nanostructures within their pores.[2-4]

Studies on the formation of porous anodic alumina from sputter-deposited aluminum layers on metal (Ta[15-18]) and semiconductor (Si[19-20]) substrates have been reported recently. They found that the anodizing process involves two stages, *i.e.*, anodization of the aluminum layer and the underlying materials (Ta or Si), and during the latter stage, the porous alumina produced in the former stage functions as a mask for a local anodization of the underlying materials, thus leading to pillared Ta_2O_5[15-16] or porous silicon nanostructures[19] with similar textures to the overlying anodic alumina. The research objectives in the studies mentioned above were concerned with structuring the substrate materials as opposed to the overlying porous anodic alumina. Consequently the anodizing process of sputtered aluminum films and the electrochemical reactions at aluminum/substrates interface have not been elucidated. Besides, many works on the anodization of Al-Zr bilayer films[21] and Al-based alloys[22] had been done to elucidate the migration of metal ions in and through the anodic oxide films. However, until now, the anodization of sputtered aluminum on conductive oxide materials (*e.g.*, indium tin oxide ITO) has not been reported.

The objective of this study was to create a novel process to fabricate transparent and porous alumina nanostructures directly on glass substrates. The porous materials can be used as hosts or templates to fabricate various nanostructures (oxides and metals) on glass,[23] for applications in photocatalysis, dye-sensitive photocells, solar energy utilization, photoelectrochemistry, magnetic nanomaterials, and so on. In the present paper, the formation process, microstructures, and the optical feature of anodic alumina films derived from aluminum sputtered on glass with an ITO film are investigated, and a possible mechanism of aluminum anodization on ITO is discussed.

Experimental

Specimens.—Highly pure aluminum (99.99%) was deposited on a soda-lime glass substrate (20 × 100 × 1.1 mm) covered with a tin-doped indium oxide (ITO) and SiO_2 films. Here, the ITO film (100-130 nm, ~20 Ω/□) was adopted as a transparent and conductive media layer to facilitate complete anodizing of aluminum metal. To the transparency of the glass materials, SiO_2 film (~15 nm) is applied to prevent sodium in glass from dispersing into the ITO film. As an additional advantage this also improves the adhesion between the ITO film and the glass substrate.

The aluminum layer (~2 μm) was produced by rf-sputtering in 2.5 deposition cycles (~0.8 μm per cycle). To guarantee the purity of the aluminum layer, a target with 99.999% purity and a higher deposition rate ~1.5 nm/s were adopted. No substrate heating or cooling was applied during the deposition. The base chamber pressure was below 1.0×10^{-5} Torr. The argon gas pressure during deposition was 2.0×10^{-3} Torr. The sputtering power was 3.5 kW, and the power density was about 2.0×10^2 kW m^{-2}.

Aluminum anodizing.—Aluminum anodizing was performed by a regulated dc power supply (Nistac) in a 10 vol % phosphoric acid solution. A phosphoric acid electrolyte was chosen because it permits anodizing at high voltages without excessive current flow and heat evolution,[14] and high voltages lead to the formation of films with a large pore diameter and cell size.[13,16]

In the experiment, the specimens were first degreased by ultrasonic-cleaning in ethanol for 10 min, and then anodized at a voltage of 130 V at 280 K. The electrolyte was mechanically stirred, and a soft increase in anodizing voltage from zero was used at the initial stage of the anodization. For reference, anodization of a highly pure aluminum sheet (JIS-1N99: 99.99%, 20 × 100 × 0.5 mm) was also performed under the same conditions. Time variation in anodic current density and voltage during anodizing was monitored by two multimeters connected with a programmed computer system.

Characterizations.—The morphology and the microstructure of the anodized specimens were observed using a field emission scanning electron microscope (FESEM: S-5000, Hitachi) with an energy dispersive X-ray analyzer (EDX). In order to minimize charging effects, the specimen was covered with a thin evaporated osmium layer. To investigate the microstructure transition of the barrier layer of anodic oxide films and the underlying ITO film, the anodic alumina films were peeled off mechanically from the substrate at the alumina-ITO interface and observed by FESEM. The crystal struc-

[z] E-mail: CHU.Songzhu@nims.go.jp

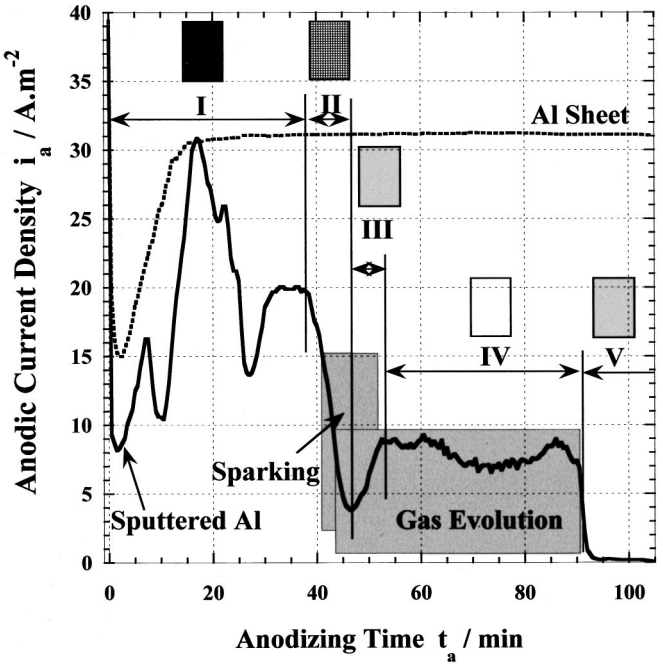

Figure 1. Changes in anodic current density (i_a) of aluminum film sputtered on glass with ITO film with anodizing time (t_a) in 10% phosphoric acid at 130 V and 280 K. The insets show the transparency of the specimens during anodizing: stage I: opaque, stage II: translucent, stage III: nearly transparent, and stage IV and V: totally transparent.

tures of the specimens were analyzed by an X-ray diffractometer (XRD: RINT-2200/PC, Cu Kα, 40 V/40 mA). The UV-visible transmittance spectra of the specimens after anodization were measured by a spectrometer (U-3500, Hitachi) at a resolution of 2 nm.

Results

Anodizing behavior.—Anodization behavior of sputtered aluminum on glass is distinct from that occurring for common aluminum sheet, since the aluminum metal is definitely consumed up through anodizing. Figure 1 shows a typical behavior of the time variation in current density (i_a-t_a) during anodizing of sputtered aluminum on glass with an ITO film in 10% phosphoric acid solution at 130 V. For reference, a current-time curve of the aluminum sheet obtained under the same conditions as the sputtered aluminum is also given in the Fig. 1 (dotted line). The anodic current density (i_a) of aluminum sheet, as usual, shows a steady value (~31 A m^{-2}) except for the initial stage. The i_a of sputtered aluminum, on the other hand, exhibits several large swings and finally goes to zero. According to the observation on the current value and the appearance (transparency) of the specimens in the experiments, the anodizing process can be divided into five stages (see the insets). In stage I, the specimens are opaque, because of the aluminum layer (inset I). The i_a varies significantly with periodic drops at t_a = 10 min and t_a = 27 min, corresponding to the deposition cycles of the aluminum layer in sputtering. The i_a value swings within 8-31 A m^{-2}, lower than that of the aluminum sheet. In stage II, the specimen changes from opaque to translucent gradually (inset II). The i_a decreases swiftly to ~3.6 A m^{-2}, accompanied with a sparking phenomenon. Entering stage III, the appearance of the specimen changes from translucent to transparent gradually (inset III). The i_a recovers gradually to a relatively low value, ~8.8 A m^{-2}, with a progressive gas evolution. In stage IV, the specimen becomes totally transparent (inset IV). The i_a varies within 6.7-8.8 A m^{-2} and lasts for a prolonged period (~40 min), accompanied by gas evolution. Approaching stage V, the i_a first experiences an increase, accompanied with a violent gas evolution, followed by a rapid decrease to zero. After the whole electrolysis is ended, the specimen remains transparent but with a slight milky white color (inset V).

Microstructure of anodic alumina film (AAF) from sputtered Al layer on glass.—The anodic current variation of sputtered aluminum on glass with ITO film corresponds to the film formation process and yield microstructural transitions within the AAF. Figure 2 shows the FESEM images of fracture sections for specimens anodized. Referring to Fig. 1, in stage I, anodizing occurs within the aluminum layer (Fig. 2a). In stage II, anodizing occurs at the interface of aluminum film and the underlying ITO film (Fig. 2b). In stage IV, all of the aluminum is electrolyzed completely into the oxide (Fig. 2c). After aluminum anodization is finished, 2 μm aluminum layers transfer to the 3 μm anodic alumina films due to the high Pilling-Bedworth ratio. The resultant anodic alumina films have a porous structure with straight and parallel channels without branches. For all the specimens, two arrays of small transverse holes appear regularly in the AAFs at the same positions (see arrows), which are ascribed to the stratified structure of sputtered aluminum layer produced in multicycled sputtering (see arrows in Fig. 2a). Figure 2d reveals the surface morphology of the AAF from sputtered aluminum layer. The AAF is composed of irregularly shaped but uniformly distributed pores with ϕ80-100 nm entrance diameter and shows little change via anodizing time.

Structure transition of barrier layer and underlying ITO film at aluminum-ITO interface.—The barrier layer of AAFs exhibits a microstructure transition during anodizing at the aluminum-ITO Interface. Figure 3 shows the FESEM images of the microstructures near the barrier layer of the films anodized at the stages of (a) within aluminum layer, (b) just reaching the underlying ITO, (c and d) nearly finishing aluminum anodizing, and (e and f) after the aluminum is fully anodized. As anodizing occurs within the aluminum layer (Fig. 3a), the barrier layer is semispherical with a thickness (~165 nm) approximately equal to half of the wall between the pores, which is consistent with conventional anodizing of bulk aluminum sheets. As the barrier layer reaches the underlying ITO layer (Fig. 3b), the aluminum under the pores is first consumed, remaining small amount of aluminum between the alumina cells (see the arrow). The frontier of the barrier layer is flat against the underlying ITO, while the inside of the barrier layer near the pores remains in semispherical shape. As anodizing goes on, the barrier layer transfers into flat in both sides (Fig. 3c) and then humps up (Fig. 3d) from the ITO/glass substrate, with a thickness of 120-147 nm. Further anodizing leads to a unique arched barrier layer with a thin thickness (~80 nm) and produces voids under each pore (Fig. 3e and f), presumably leading to a weak connection with the substrate. Moreover, it should be noticed in Fig. 3f that there are several black lines across the barrier layer adjacent to the porewalls (see arrows), which could correspond to some of the tiny pores in the barrier layer (refer to Fig. 4b).

Figure 4 shows the FESEM images from the bottom view of the barrier layers of anodic alumina films (left photos) and the surface morphology of the corresponding underlying ITO film (right photos) for the specimens anodized for (a) and (b) t_a = 50 min, (c and d) t_a=60 min, and (e and f) t_a = 105 min. For the specimen anodized for 50 min (Fig. 4a), *i.e.*, when the aluminum is almost fully anodized into the oxide, the barrier layer is basically dense with shallow dents. Some tiny pores can be seen at the grain boundaries of the aluminum or the alumina (arrows A). Correspondingly, the underlying ITO film (Fig. 4b) is an even layer with numerous tiny pillars, similar to that without anodizing (not show), though some dark regions (arrows A) indicate the effect from the anodizing. As the aluminum is completely anodized (Fig. 4c), numerous tiny pores (arrows A) appear around the barrier layer at the pore base. The dents corresponding to the arched barrier layer are deeper topographically than those in Fig. 4a, inferring a thinner barrier layer, which is consistent with Fig. 3e and f. On the other hand, the correspond-

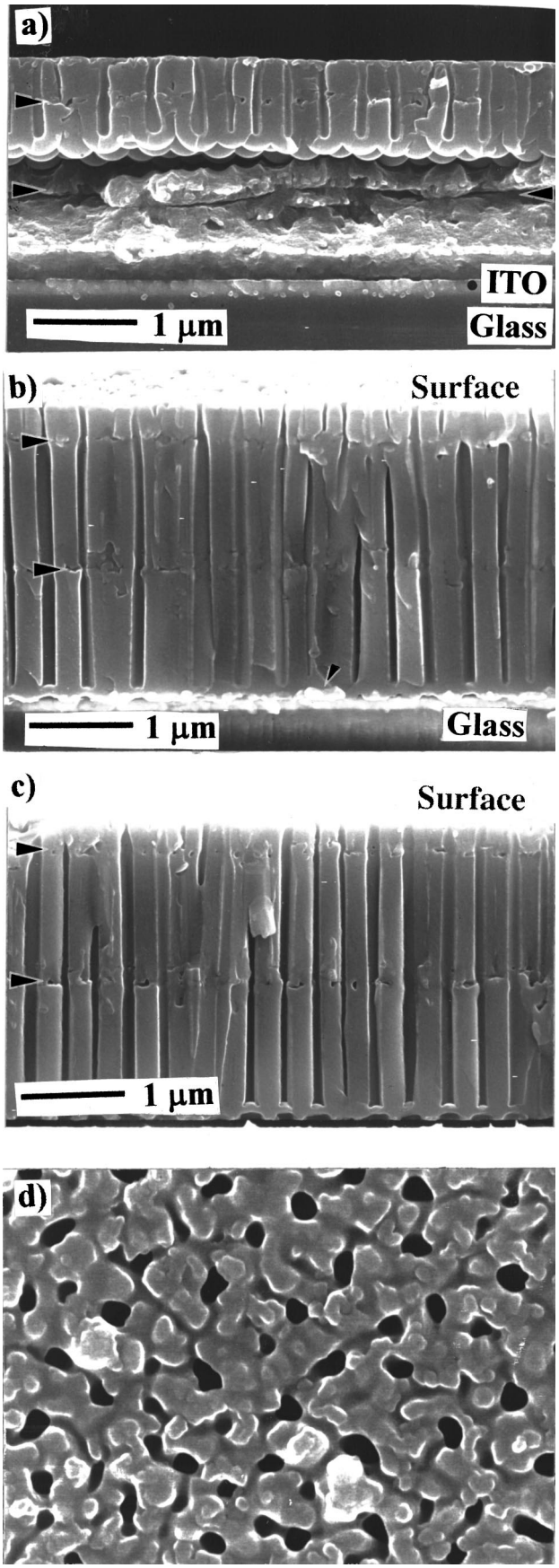

Figure 2. Field-emission scanning electron microscope (FESEM) images of fracture sections for anodized specimens: (a) stage I: t_a = 16 min, (b) stage II: t_a = 46 min, (c) stage IV: t_a = 60 min, and (d) surface morphology of (c).

ing ITO film (Fig. 4d) is still a continuous layer but with a partly uneven surface. Some dark circles (arrows) with the same dimensions and spacing as those in Fig. 4c are observed and identified as dents from the topography. Finally, for the specimen obtained after the anodic current goes to zero (Fig. 4e), the barrier layer still exists but becomes a flat one, and in addition to the tiny pores (arrows A), local perforation of the barrier layer also occurs in many places (arrows B). Accordingly, the underlying ITO film (Fig. 4f) has become a discontinuous one, exposing the glass substrate (regions B) and giving a poor adhesion between the film and the substrate. From the enlarged image of remnant ITO film (inset in Fig. 4f), the tiny pillars on the surface of ITO film have almost disappeared, and some holes (arrows A) with the same dimensions to the dents in Fig. 4d are observed.

Moreover, it was found by EDX analysis that no difference in the compositions was detected between the pore walls and pore bases (Fig. 4a, c, and e) and between the flat region and the dark circles on the ITO film (Fig. 4d). Additionally, a small amount (~1 wt%) of indium was detected in the bright regions in Fig. 4f apart from the aluminum, oxygen, and phosphorus in anodic alumina, indicating the peeling of anodic alumina films happened at the interface between anodic alumina and ITO films.

X-ray diffraction (XRD) analysis.—Figure 5 gives the results of XRD analysis for specimens before and after anodizing at different time. The sputtered aluminum layer (a) is polycrystalline with strong orientation in (111) facet, which is different from the common metallurgical aluminum sheet with preferential (200) orientation. In addition to the peaks of metallic aluminum, the peaks corresponding to the indium oxide from the underlying ITO film on glass substrates also appear, due to the limited thickness of the aluminum layer. After the aluminum is fully anodized into the oxide (b), the main peak in (111) orientation corresponding to metallic aluminum disappears completely. No peak corresponding to crystallized Al_2O_3 is found, though sparking has occurred during the ending stage of aluminum anodizing, indicating that the anodic aluminum oxide is still amorphous as anticipated. All the peaks in pattern b are identified as the indium oxide from the ITO films beneath the anodic alumina film. No phases associated with tin were detected, most likely due to the low total tin content in the ITO. As for the specimen anodized for 105 min (c), only a weak peak at 30.1° (main peak of In_2O_3) appears, due to the discontinuous ITO film (see Fig. 4f). Moreover, from the peak positions of In_2O_3 for all specimens, it could be deduced that the crystal structure of the indium oxide is not affected by the electrolysis.

Transparency of anodic alumina films.—The transmittance of anodic oxide films on glass substrates is an important parameter in making devices for photochemical applications. Figure 6 illustrates the UV-visible transmittance spectra for the specimens after anodizing for different times. The sputtered aluminum layer without anodizing is opaque (broken line). As anodizing proceeds down to aluminum/ITO interface (t_a = 38 min), the specimen becomes translucent gradually due to the thinning of aluminum metal layer. With the consumption of remnant aluminum metal by anodizing, the transparency of the specimens increases gradually, and the interference in the spectra becomes strong simultaneously. The interference in the transmittance spectra could be ascribed to the thickness and the porous structure of anodic alumina films, as well as the refractive index of the ITO film (100-130 nm; 2.0) and the SiO_2 film (~15 nm; 1.4). As the aluminum is completely converted into the oxide (stage IV: t_a = 60 min), the average transmittance of the anodic alumina film in visible light range reaches to ~95%. Further electrolyzing the specimens until the current goes to zero (stage V: t_a= 105 min) results in lowering of transmittance (dotted line), possibly due to the diffusion of light from the rough and discrete ITO film (see Fig. 4f). In other words, the transmittance of the specimens corresponds to the consumption of aluminum during an-

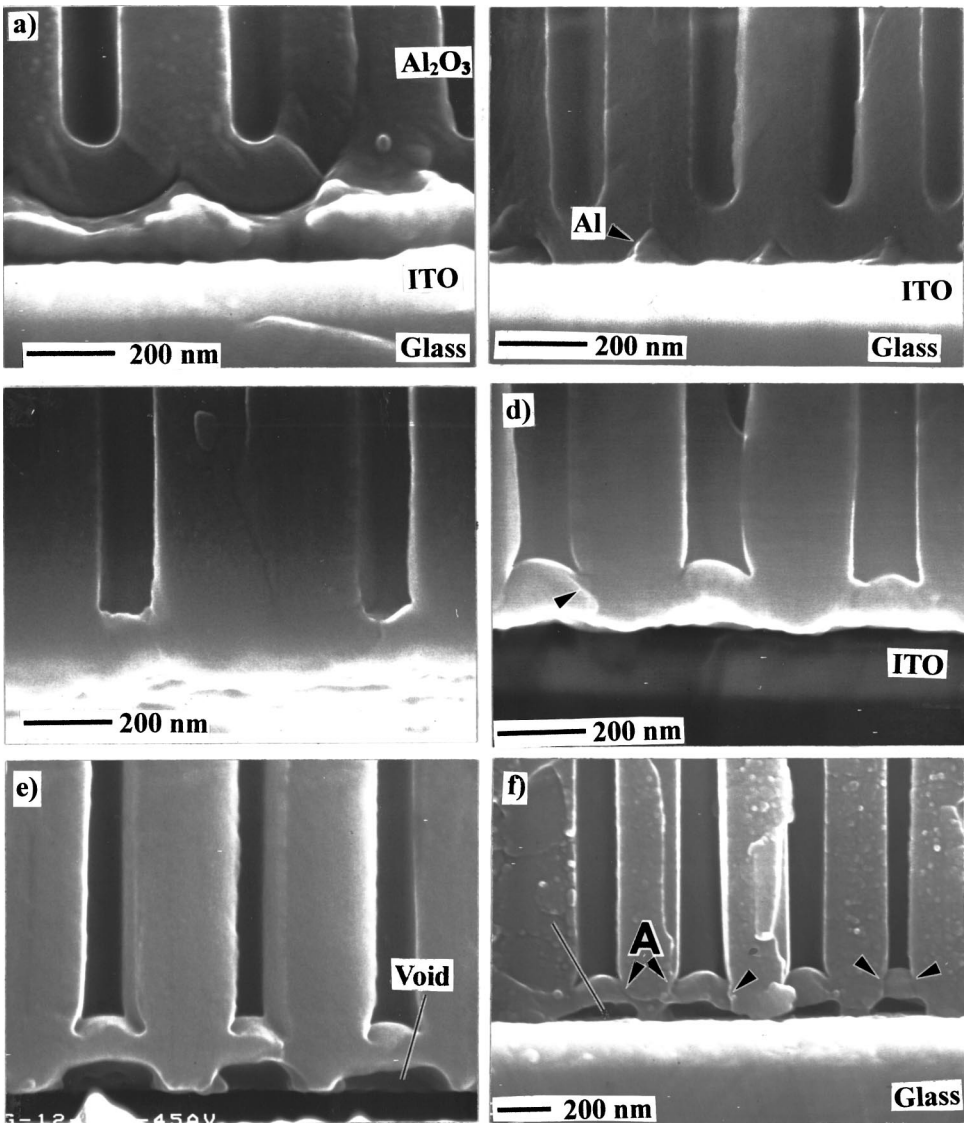

Figure 3. High-resolution FESEM images of fracture sections near the barrier layer of anodic alumina for the specimens anodized for (a) stage I: t_a = 38 min, (b) stage II : t_a = 45 min, (c) stage III: t_a = 50 min, (d) stage III: t_a = 53 min, and (e and f) stage IV: t_a = 60 min.

odizing. Therefore, the transparency of the specimen could be used as another indicator for the termination of aluminum anodizing in addition to the current variation.

Discussion

The anodizing behavior of the superimposed metal/oxide layers is complex, and may be distinct from those of metallic layers.[16-19,21] In the present study, the anodizing of the superimposed aluminum and ITO layers on glass involves three main processes as follows

(i). Aluminum anodizing within the sputtered aluminum layer (stage I in Fig. 1): Generally, anodic oxide films on aluminum, independent of barrier type or porous type, are formed by the simultaneous outward migration of Al^{3+} and inward O^{2-}/OH^- ions. The ions are driven by the high applied electric field, across a compact layer of film material (*i.e.*, barrier layer) at the aluminum-film interface, according to following reactions[6,24-28]

$$Al = Al^{3+} + 3e \quad [1]$$

$$2Al^{3+} + 3H_2O = Al_2O_3 + 6H^+ \quad [2]$$

$$2Al + 3O^{2-} = Al_2O_3 + 6e \quad [3]$$

Reaction 1 contributes to the most of the anodic current, and Reactions 2 and 3 relate to the growth of the anodic oxide film and the generation of hydrogen ions as a by-product. In the present study, since the anodizing conditions (electrolyte, temperature, voltage, etc.) are fixed, the value and variation of the anodic current mainly depended on the property of the electrode materials. The anodic current of sputtered aluminum (16-31 A m^{-2}) is lower than that of aluminum sheet (~32 A m^{-2}), and varies with the deposition history of the layer (Fig. 1). In particular, the sputtered aluminum used in this study possesses a stratified structure as a result of the multicycled deposition used in sputtering (Fig. 2a). Consequently, the anodizing progress of sputtered aluminum is disrupted or hindered at the interface zones between the deposited aluminum layers (per cycle). This is reflected in the transient decrease of the current density (Fig. 1) and the formation of the transverse holes (Fig. 2). Nevertheless, the pores of the resultant anodic alumina films grow straight and run through the interface zones regardless of the stratified structure of sputtered aluminum layer, leading to an entirely porous structure. This characteristic is essential when seeking to grow thicker anodic alumina films from sputtered aluminum layer.

(ii). Transition of electrolysis from anodizing of sputtered aluminum to underlying ITO (stage II and III in Fig. 1): The transition of anodizing the aluminum film to the underlying ITO is characterized by current variation(s), accompanied by an apparent transparency change. The current fluctuation in stage II and III indicates that at least two electrochemical processes are involved, *i.e.*, aluminum anodizing (Reactions 1 and 3) and electrolysis on ITO (*e.g.*, Reactions 4 and 5). As the barrier layer reaches the substrate gradually (Fig.

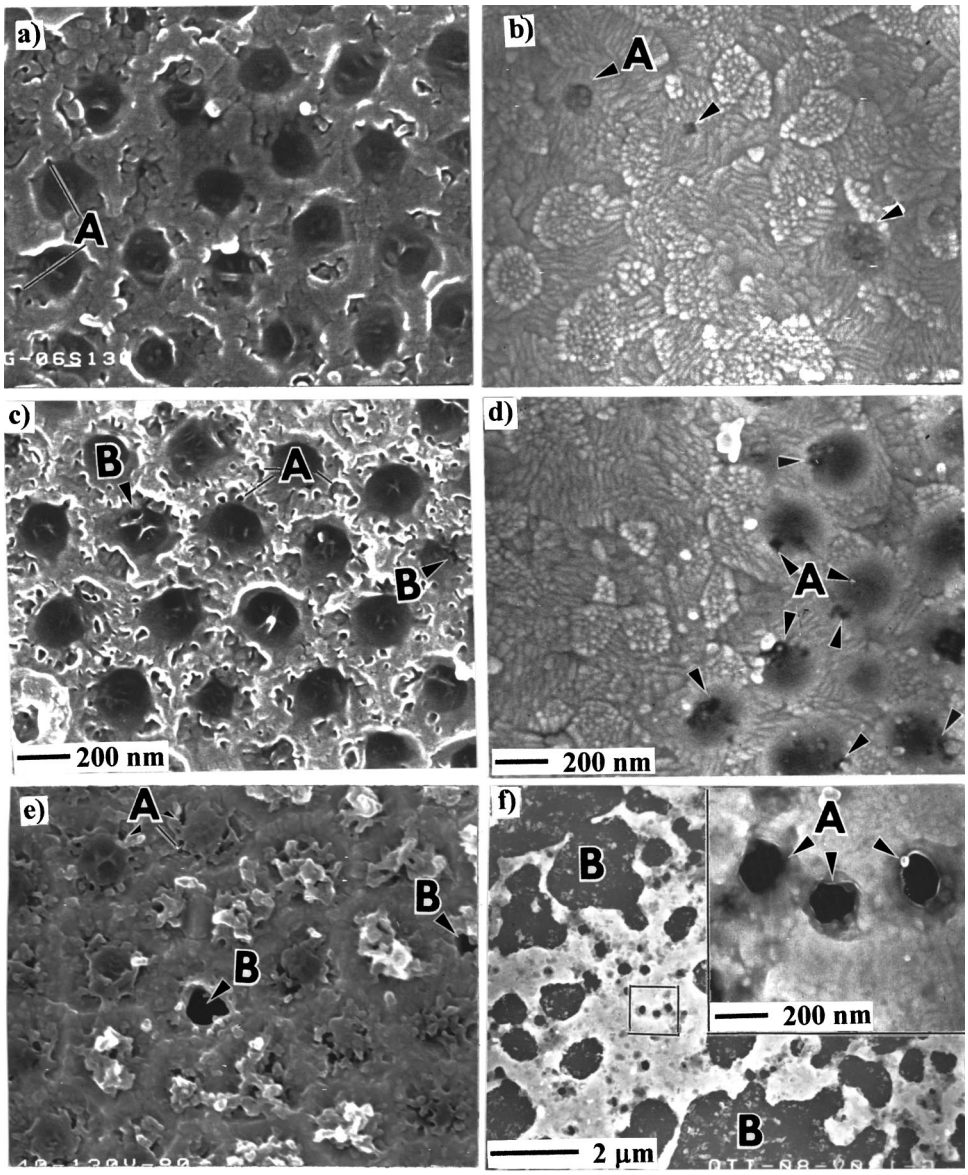

Figure 4. FESEM images from the bottom view of the barrier layers of anodic alumina films (left photos) and the surface morphology of the corresponding underlying ITO film (right photos) for the specimens anodized for (a) and (b) t_a = 50 min, (c) and (d) t_a = 60 min, and (e) and (f) t_a = 105 min. Inset in (f) is the high magnification image of (f) within the square area. The bright regions in f) correspond to ITO film, and dark regions to the glass substrate.

3b), the area and the amount of aluminum metal reduce abruptly, so the current corresponding to aluminum anodizing through Reaction 1 decreases accordingly (stage II). Meanwhile, the electrolysis would gradually be dominated by processes occurring at the underlying ITO film (see later discussion). This results in the transient current drop which marks the completion of aluminum anodization.

During the transition process, the barrier layer changes from semispherical to flat, and finally to arched (Fig. 3b-e). The formation of the humped or arched barrier layer may be ascribed to the anodizing of remnant aluminum, during which a certain thickness corresponding to the applied voltage should be maintained, and more possibly, to the oxygen at the alumina-ITO interface produced through the following reaction[28]

$$2\,O^{2-} = O_2 + 4e \qquad [4]$$

As anodization proceeds in the aluminum layer, oxygen is not produced at the Al-alumina interface, since the equilibrium potential of Reaction 3 is less than that of Reaction 4. However, as the barrier layer reaches the ITO film, the O^{2-} ions delivered to the alumina-ITO interface via barrier layer may react with either aluminum or ITO. Assuming that the ITO just functions as an electrochemical inert electrode, oxygen would be produced through Reaction 4 and accumulated at the alumina/ITO interface. This would produce a pressure against the pore base, so high that would lift up the barrier layer from the interface and leave some voids beneath the barrier layer (Figs. 3d-f), thus leading to a weak connection between the alumina film and the ITO/glass substrate (Figs. 4a and c).

It is interesting that numerous tiny pores are formed at the barrier layer adjacent to pore walls at the end of aluminum anodizing (arrows A in Fig. 4a, c, and e). The formation mechanism of the tiny pores is not clear. It could be ascribed to the combined effect of local anodization of the remnant aluminum around the pores walls and the high-pressure oxygen produced through Reaction 4. Some of the tiny pores might penetrate the barrier layer for some reasons (arrows A in Fig. 3d), thus permit the electrolyte reaching the alumina-ITO interface, leading to the local dissolution of the underlying ITO film (black circles in Fig. 4d). The black dots at the edges of black circles in Fig. 4d might be the initial points of dissolution. The perforation of the barrier layer leads to a current rise corresponding to the current recovering in stage III in Fig. 1, in which the current value is depended on the extent of the perforation, the conductivity of the ITO film, electrolyte used, and so on. Here, a massive rise in current was not observed, indicating that the perforation of the barrier layer might proceed gradually and very slowly.

The variation in the barrier layer thickness during anodizing at

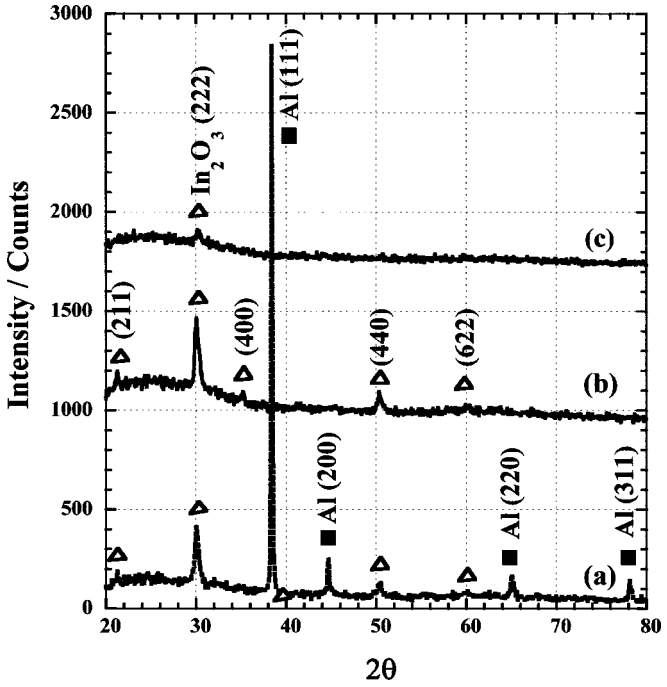

Figure 5. X-ray diffraction patterns of (a) sputtered aluminum, and anodic alumina films of (b) $t_a = 50$ min, and (c) $t_a = 105$ min on a glass substrate with an ITO film. (Cu Kα, 40 mA/40 V).

the alumina/ITO interface is another interesting phenomenon during the transition. As anodizing occurs in the aluminum layer (Fig. 3a), the thickness of the barrier layer in semisphere is approximately 165 nm, equivalent to 1.27 nm/V. This value is consistent with that of conventional anodizing of bulk aluminum sheets, which is usually 1.0-1.4 nm/V. While after the aluminum is completely anodized (Fig. 3e), the barrier layer thickness is ~80 nm, equivalent to 0.62 nm/V, which is unusually thin for alumina films anodized at such a high voltage. The reason for the reduction in barrier layer thickness is uncertain due to the limited data. It could be ascribed to either the sparking at the end of aluminum anodizing, in which the dehydration or crystallization of the barrier layer of anodic alumina could be induced, though could not detected by the XRD analysis (Fig. 5), or the chemical dissolution at the alumina/ITO interface caused by the localized increase of temperature due to the highly resistive underlying ITO film on glass,[19] or both.

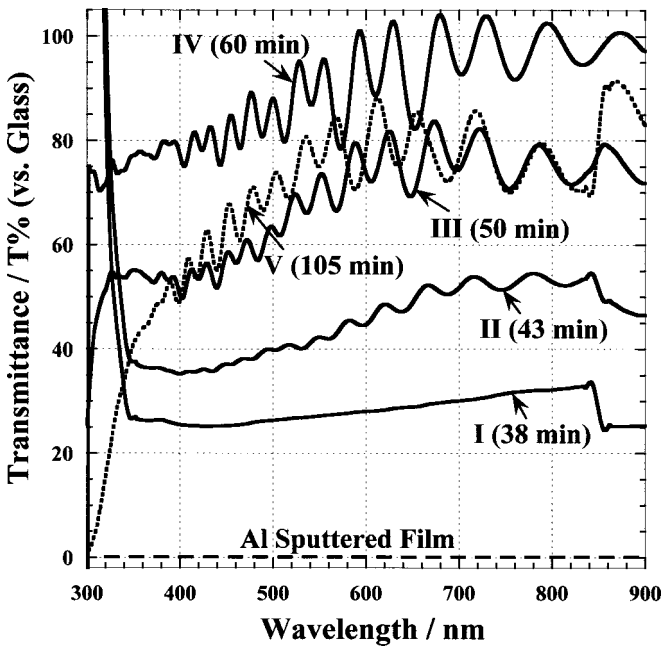

Figure 6. UV-visible transmittance spectra of specimens anodized for different times. A glass plate with an ITO film was used as a reference sample.

(iii). Electrochemical reactions on ITO film (stage IV in Fig. 1):

A quite possible electrochemical reaction contributing to the current and gas evolution in stage III and IV may be the electrolysis of water in the electrolyte at the alumina-ITO interface through the tiny pores of the barrier layer

$$2H_2O_2 = O_2 + 4H^+ + 4e \quad E° = +1.229 \text{ V} \qquad [5]$$

It can be derived from the standard potential that oxygen generation is quite possible through Reaction 5 at the high applied voltage (130 V). The resulting oxygen would escape from the alumina ITO interface through the pores, accounting for the gas evolution observed in the experiment. The resulting hydrogen ions would cause a local acidification of the electrolyte, and lead to a local dissolution of the underlying ITO film (dents in Fig. 4d and f), enhanced by the high electric field of 130 V. Here, anodic dissolution of the ITO film may occur nonuniformly and very slowly through the tiny pores of the overlying anodic alumina film. This may be the reason why the current in stage IV goes on for a prolonged period in spite of the limited thickness of the ITO film (100-130 nm). The local acidification of the electrolyte would also cause the dissolution of the overlying barrier layer and result in the void formation at the alumina-ITO interface (Fig. 3f), leading to a poor adhesion between the alumina film and the substrate. Particularly, as the breakdown of the barrier layer occurs (see arrows B in Fig. 4e), large volume electrolyte would "pour" in the alumina/ITO interface and promote Reaction 5, which probably contributes to the current increase and violent gas evolution near the end of stage IV. Eventually, the ITO film would be corroded into discrete islands (Fig. 4f), and the anodic current decreases to zero (stage V in Fig. 1).

Finally, it should be mentioned that the electrochemical reactions of the ITO film after consumption of aluminum have largely been neglected in the above discussion. Speculatively, the ITO could also participate in electrochemical reactions, in dissolution and/or oxidation form. For instance, though without any direct evidence, part of the indium ions could migrate into the barrier layer of anodic alumina due the higher mobility,[29,30] driven by the high applied voltage. This would change the oxide composition at the pore base and increase its field strength. Such an effect, like the sparking effect mentioned before, might also account for some of the reduction in barrier layer thickness. However, to elucidate the electrochemical behavior of the ITO film beneath anodic alumina, more accurate analysis and further investigations are needed and will be no longer elaborated in present paper.

Conclusions

Nanostructures of transparent porous anodic alumina films are formed directly on a glass substrate with an ITO film through the anodization of sputter-deposited aluminum layer. The anodic alumina films are composed of straight and parallel nanopores with a thin arched barrier layer and transverse holes, and exhibit a high transmittance in the UV-visible light range, due to the complete anodizing of aluminum.

The anodizing process of sputtered aluminum on glass with a conductive ITO film involves three major stages

(i) anodization of the sputtered aluminum layer, exhibiting a dependence of current variation upon the deposition conditions;

(ii) transition from anodization of aluminum to electrolysis involving the underlying ITO film, during which the anodic current density experiences a transient decrease and recovers to a relatively

low value, and the specimens change from opaque to transparent simultaneously, accompanied with sparking and gas evolution;

(iii) electrochemical reactions, *e.g.*, decomposition of water, on the ITO film beneath the anodic alumina films, leading to a discrete ITO film segment and a loss of electrode conductivity.

Therefore, by stopping the anodization promptly after the characteristic current variation is detected and the transparency change of the specimen is observed, a transparent porous electrode material with good conductivity and large surface area can be obtained for various practical purposes.

Acknowledgments

This work is part of the Japan Millennium Project of ''Search and Creation of a Catalyst for Removing Harmful Chemical Substances.'' The authors wish to thank the Asahi Glass Co., Ltd for providing glass substrates with ITO films and Kyodo International Company for assisting aluminum sputtering.

The National Institute for Materials Science assisted in meeting the publication costs of this article.

References

1. A. Huczko, *Appl. Phys.*, **70**, 365 (2000).
2. T. Kyotani, B. K. Pradhan, and A. Tomita, *Bull. Chem. Soc. Jpn.*, **72**, 1957 (1999).
3. M. Zhang, Y. Bando, K. Wada, and K. Kurashima, *J. Mater. Sci. Lett.*, **18**, 1911 (1999).
4. B. B. Lakshmi, P. K. Dorhout, and C. R. Martin, *Chem. Mater.*, **9**, 857 (1997).
5. H. Masuda and K. Fukuda, *Science*, **268**, 1466 (1995).
6. S. Wernick, R. Pinner, and P. C. Sheasby, *The Surface Treatment and Finishing of Aluminum and Its Alloys*, ASM International, Metals Park, Ohio, U.S.A, Finishing Publications Ltd., Teddington, Middlesex, England (1987).
7. G. E. Thompson and G. C. Wood, *Treatise on Materials Science and Technology*; C. Scully, Editor, Academic Press, New York (1983).
8. H. Takahashi, M. Nagayama, H. Akahori, and A. Kitahara, *J. Electron Microsc.*, **22**, 149 (1973).
9. H. Takahashi, J. Yamada, and M. Nagayama, *Metal Surface Finishing of Jpn.*, **28**, 286 (1977).
10. K. Wada, T. Shimohira, M. Yamada, and N. Baba, *J. Mater. Sci.*, **21**, 3810 (1986).
11. O. Jessensky, F. Müller, and U. Gösele, *J. Electrochem. Soc.*, **145**, 3735 (1998).
12. H. Masuda and F. Hasegawa, *J. Electrochem. Soc.*, **144**, L127 (1997).
13. H. Masuda, H. Yamada, M. Satoh, and H. Asoh, *Appl. Phys. Lett.*, **71**, 2770 (1997).
14. R. C. Furneaux, W. R. Ribgy, and A. P. Davidson, *Nature (London)*, **337**, 147 (1989).
15. A. I. Vorobyova and E. A. Outkina, *Thin Solid Films*, **1-10**, 324 (1998).
16. A. Mozalev, A. Surganov, and S. Magaino, *Electrochim. Acta*, **44**, 3891 (1999).
17. A. Mozalev, A. Poznyak, I. Mozaleva, and A. W. Hassel, *Electrochem. Commun.* **3**, 299 (2001).
18. A. Mozalev, A. Surganov, and H. Imai, *Electrochim. Acta*, **46**, 2825 (2001).
19. D. Crouse, Y. Lo, A. E. Miller, and M. Crouse, *Appl. Phys. Lett.*, **76**, 49 (2000).
20. J. Zou, J. Wu, Q. Zhu, L. Pu, J. Zhu, and X. Bao, *Bandaoti Xuebao*, **21**, 255 (2000).
21. K. Shimizu, K. Kobayashi, P. Skeldon, G. E. Thompson, Y. Xu, and G. C. Wood, *Thin Solid Films*, **295**, 156 (1997).
22. H. Habazaki, K. Shimizu, P. Skeldon, G. E. Thompson, and G. C. Wood, *Philos. Mag. A*, **73**, 445 (1996).
23. S. Z. Chu, K. Wada, S. Inoue, and S. Todoroki, *Chem. Mater.* **14**, 266 (2002).
24. G. E. Thompson, Y. Xu, P. Skeldon, K. Shimizu, S. H. Han, and G. C. Wood, *Philos. Mag. A*, **55**, 651 (1987).
25. G. Patermarakis and K. Moussoutzanis, *Electrochim. Acta*, **40**, 699 (1995).
26. H. Takahashi, K. Fujimoto, K. Konno, and M. Nagayama, *J. Electrochem. Soc.*, **131**, 1856 (1984).
27. F. Li, L. Zhang, and R. M. Mewtzger, *Chem. Mater.*, **10**, 2470 (1998).
28. P. Skeldon, G. E. Thompson, G. C. Wood, X. Zhou, H. Habazaki, and K. Shimizu, *Philos. Mag. A*, **76**, 729 (1997).
29. I. Felhosi, H. Habazaki, K. Shimizu, P. Skeldon, G. E. Thompson, G. C. Wood, and X. Zhou, *Corros. Sci.*, **40**, 2125 (1998).
30. A. Pakes, F. Echeverria, P. Skeldon, G. E. Thompson, J. W. Fraser, J. P. McCaffrey, S. Moisa, M. J. Graham, H. Habazaki, and K. Shimizu, *Corros. Sci.*, **43**, 2173 (2001).